Volatile loss following cooling and accretion of the Moon revealed by chromium isotopes

Paolo A. Sossi[a,1], Frédéric Moynier[a,b], and Kirsten van Zuilen[a,2]

[a]Institut de Physique du Globe de Paris, Université Paris Diderot, Université Sorbonne Paris Cité, CNRS UMR 7154, 75238 Paris Cedex 05, France; and [b]Institut Universitaire de France, 75231 Paris Cedex 05, France

Terrestrial and lunar rocks share chemical and isotopic similarities in refractory elements, suggestive of a common precursor. By contrast, the marked depletion of volatile elements in lunar rocks together with their enrichment in heavy isotopes compared with Earth's mantle suggests that the Moon underwent evaporative loss of volatiles. However, whether equilibrium prevailed during evaporation and, if so, at what conditions (temperature, pressure, and oxygen fugacity) remain unconstrained. Chromium may shed light on this question, as it has several thermodynamically stable, oxidized gas species that can distinguish between kinetic and equilibrium regimes. Here, we present high-precision Cr isotope measurements in terrestrial and lunar rocks that reveal an enrichment in the lighter isotopes of Cr in the Moon compared with Earth's mantle by 100 ± 40 ppm per atomic mass unit. This observation is consistent with Cr partitioning into an oxygen-rich vapor phase in equilibrium with the proto-Moon, thereby stabilizing the CrO_2 species that is isotopically heavy compared with CrO in a lunar melt. Temperatures of 1,600–1,800 K and oxygen fugacities near the fayalite–magnetite–quartz buffer are required to explain the elemental and isotopic difference of Cr between Earth's mantle and the Moon. These temperatures are far lower than modeled in the aftermath of a giant impact, implying that volatile loss did not occur contemporaneously with impact but following cooling and accretion of the Moon.

Moon | chromium | evaporation | low temperature | equilibrium

The volatile-depleted nature of the Moon was recognized upon analysis of the first lunar samples returned by the Apollo missions (1), yet it remains one of its most enigmatic characteristics (2, 3). The gross depletions in volatile elements in the lunar mantle relative to Earth's stand in contrast to the chemical and isotopic similarity observed for refractory elements (4–6). Although some models account for this accord by a giant impact in which the impactor had an isotopic composition identical to that of Earth (7), this explanation cannot account for the impoverishment of Cr, Mn, and V in the lunar mantle. The depletion in these elements in both the lunar and terrestrial mantles relative to other solar system bodies uniquely resulted from the high pressure under which Earth's core formed (8–10) and constitutes strong evidence for the derivation of the Moon from Earth's mantle (4).

Within this genetic framework, however, the thermochemical conditions that could engender similarity in refractory lithophile element abundances yet strong volatile element depletion in the Moon remain poorly understood. Based on the observation that lunar mare basalts are depleted only in elements more volatile than Li (e.g., ref. 11), temperatures of ∼1,100 K for lunar volatile loss have been proposed (2, 12), reflecting the nebular half-condensation temperature of Li. However, this conclusion is contingent upon the assumption that element volatility during condensation of the solar nebula is transferable to that for evaporation of lunar silicates. Equilibrium thermodynamic calculations provide grounds to reject this assumption, as the vapor calculated to be in equilibrium with a model lunar mantle composition has oxygen fugacities orders of magnitude higher (13, 14) than in the solar nebula. These thermodynamic variables affect element volatility, and new dynamical simulations invoke higher temperatures (>2,500 K) to simultaneously reproduce lunar volatile depletion in the Earth–Moon disk and equilibrate refractory elements between the two bodies (14, 15).

Stable isotopes can shed light on these discrepant temperature estimates because, at equilibrium, their fractionation between two phases (e.g., liquid and gas) is proportional to $1/T^2$. The enrichment in the heavier isotopes of Zn, K, Rb, Ga, and Cl in lunar rocks relative to Earth's mantle attests to their evaporation and subsequent escape from the Moon (16–21). Whether this loss occurred during local magmatic degassing (20, 22), a magma ocean phase (17, 23, 24), or following a giant impact (1, 16) remains debated. Determining the conditions of volatile depletion, therefore, has the potential to distinguish between these scenarios. However, it has been hitherto impossible to quantify evaporation temperatures by using the isotope compositions of Zn, K, Ga, and Rb, because their vapor species are monatomic gases (e.g., Zn^0) (25), which favor the lighter isotopes with respect to the condensed phase (e.g., ZnO) (26). As such, the direction of isotopic fractionation is the same, be it at equilibrium or during kinetic vapor loss into a vacuum, for which the fractionation factor is temperature-independent. Chromium represents a special case; although $Cr^0_{(g)}$ is stable in the solar nebula, unlike the aforementioned elements, it also has several oxidized gas species, namely, $CrO_{(g)}$, $CrO_{2(g)}$, and $CrO_{3(g)}$ (27). Therefore, under the more oxidized conditions that typify evaporation of planetary mantles (13), Cr becomes more volatile, whereas other moderately volatile elements (e.g., Rb and Zn) become

Significance

With the exception of volatile elements, which are strongly depleted and isotopically fractionated, the Moon has chemical and isotopic signatures that are indistinguishable from Earth's mantle. Reconciliation of these properties with Moon formation in a high-energy giant impact invokes evaporative loss of volatile elements, but at conditions that are poorly known. Chromium isotopic fractionation is sensitive to temperature variations and liquid–gas equilibration during evaporation. We measure an isotopic difference between Earth's mantle and the Moon, consistent with the loss of a Cr-bearing, oxidized vapor phase in equilibrium with the proto-Moon. Temperatures of vapor loss required are much lower than predicted by recent models, implying that volatile elements were removed from the Moon following cooling rather than during a giant impact.

less so. As such, evaporative loss of Cr is possible under these conditions (11) and could engender light isotope enrichment in the residue.

To evaluate whether there are any Cr isotope differences between Earth and the Moon, 17 spinifex-textured komatiites, whose compositions approximate those of liquids, were sourced from five different cratons (28). These samples constitute records of Earth's mantle composition in the Archean, and together with three modern peridotites, they are used to estimate its Cr isotope composition through time and space. Estimates of the Moon's composition were garnered by analysis of six Mg-Suite samples, a set of cogenetic cumulate rocks that record the early stages of the Moon's differentiation (29), in addition to five lunar mare basalts and lunar green glass. The Cr isotopic data are reported as $\delta^{53}Cr$, the per-mille deviation of the $^{53}Cr/^{52}Cr$ ratio of the sample from the National Institute of Standards and Technology (NIST) Standard Reference Materials (SRM) 979 standard, together with its associated 2SD uncertainty throughout, unless otherwise specified.

Twenty terrestrial ultramafic samples have $\delta^{53}Cr$ between -0.17 ± 0.06‰ (sample 422/95) and -0.07 ± 0.04‰ (sample 49J), with an average of -0.11 ± 0.05‰ (Table 1), identical to the average of samples used to define bulk silicate Earth (BSE), -0.13 ± 0.10‰ (30), but less scatter. The lack of isotopic variation despite differences in (i) different emplacement ages [3.5–2.7 gigaannum (Ga) for komatiites; present-day for peridotites], (ii) komatiite source fertility, and (iii) lithology

Table 1. Chromium isotopic composition, chromium content, and MgO content of samples

Sample	Rock type	$\delta^{53}Cr$, ‰	2×SD	n	Cr, ppm	MgO, wt%
Earth						
49J	Komatiite	−0.065	0.041	3	3,190	32.16
B-R1	Komatiite	−0.155	0.035	3	2,650	27.72
179/751	Komatiite	−0.122	0.066	3	3,240	23.54
176/723	Komatiite	−0.122	0.048	3	2,450	31.13
SD5/354.5	Komatiite	−0.121	0.017	2	3,050	25.72
331/783	Komatiite	−0.082	0.039	3	2,894	26.69
331/777A	Komatiite	−0.114	0.012	2	2,717	26.26
422/94	Komatiite	−0.147	0.035	2	3,464	22.41
422/95	Komatiite	−0.168	0.059	2	3,260	23.45
422/84	Komatiite	−0.112	0.004	2	2,902	30.32
RL-12–1	Kom. basalt	−0.111	0.010	2	1,351	13.68
331/790	Px. cumulate	−0.132	0.006	2	3,371	16.05
422/96	Komatiite	−0.097	0.001	2	3,060	28.71
SD6/400	Komatiite	−0.098	0.004	2	2,428	27.99
422/96a	Komatiite	−0.085	0.001	2	3,060	28.71
331/948	Komatiite	−0.104	0.004	2	2,915	23.54
331/779	Komatiite	−0.097	0.004	2	2,706	26.76
DTS-1	Dunite	−0.127	0.007	2	3,990	49.59
PCC-1	Harzburgite	−0.083	0.004	2	2,730	43.43
DTS-1a	Dunite	−0.123	0.003	2	3,990	49.59
Moon						
15445	Norite	−0.082	0.007	2	1,635	10.20
15455	Norite	−0.116	0.009	2	810	10.90
76535	Troctolite	−0.253	0.005	2	753	19.09
78235	Norite	−0.140	0.003	2	1,500	11.76
78328	Norite	−0.138	0.006	2	1,500	11.76
72415	Dunite	−0.297	0.011	2	2,414	43.61
15555	Low Ti	−0.283	0.004	2	4,290	11.10
12002	Low Ti	−0.234	0.009	2	5,949	14.82
15426	Green glass	−0.186	0.009	2	3,557	17.50
10003	High Ti	−0.307	0.007	2	1,583	7.10
70135	High Ti	−0.196	0.012	2	3,921	9.30
10057	High Ti	−0.243	0.002	2	2,303	7.60

n denotes the number of replicates on the MC-ICP-MS. Kom., komatiitic; Px., pyroxene.

(peridotites vs. komatiites) attests to the homogeneity of Cr isotopes in convecting mantle from 3.5 Ga to the present day. The Cr isotope compositions for the five mare basalts range from -0.31 ± 0.01‰ in sample 10003 to -0.20 ± 0.01‰ in sample 70135, both of which are high-Ti basalts and span the range of the two low-Ti basalts (Table 1). A previous study found overlapping Cr isotope compositions in low- and high-Ti basalts, with an average of -0.22 ± 0.10‰ (31). As a whole, lunar mare basalts tend to lighter $\delta^{53}Cr$ with decreasing Cr (Fig. 1A) and MgO content (Fig. 1B). By contrast, the Mg-Suite cumulates record an increase of $\delta^{53}Cr$ with falling MgO (Fig. 1B). The olivine-rich samples dunite 72415 and troctolite 76535 have $\delta^{53}Cr$ within the range of lunar mare basalts (-0.30 ± 0.01‰ and -0.25 ± 0.01‰, respectively), while the more evolved norites (orthopyroxene-plagioclase) have distinctly heavier compositions, up to -0.08 ± 0.01‰. Green glass clods from soil sample 15426 have $\delta^{53}Cr = -0.19 \pm 0.01$‰.

Mechanics of Cr Isotope Fractionation During Magmatic Processes

Chromium isotope fractionation arises from the decoupling of Cr^{2+} and Cr^{3+} in magmatic phases. Their relative abundance in silicate liquids is dependent on oxygen fugacity, fO_2, according to the homogeneous equilibrium:

$$CrO_{1.5} = CrO + \frac{1}{4}O_2. \qquad [1]$$
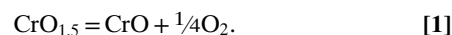
The positive entropy change of reaction (Eq. 1) stabilizes chromous oxide to high temperatures (32). Terrestrial and lunar magmas have fO_2 near the fayalite–magnetite–quartz (FMQ) and ~1 log unit below the iron–wüstite (IW) buffers, respectively (33). Under these conditions with $\log K_{(1)} \sim 1.9$ at 1,400 °C, $Cr^{2+}/\sum Cr$ is 0.32 and 0.91 for terrestrial and lunar magmatic liquids, respectively (34).

In (ultra)mafic magmas, olivine, pyroxene, and chromite can leverage Cr isotope fractionation in the liquid from which they crystallize. The precipitation of chromite, $(Fe,Mg)Cr^{3+}_2O_4$, is favored by increasing fO_2 and falling temperature that increase $aCrO_{1.5}$ in the liquid (Eq. 1, ref. 35). Although chromite saturation occurs with olivine in some komatiitic magmas, its effect on the Cr isotope composition of the samples measured is negligible, owing to (i) the high temperatures, >1,450 °C (36); (ii) the fact that they represent quenched liquids and have not undergone chromite accumulation or fractionation; and (iii) the high fO_2 and hence Cr^{3+} content of terrestrial melts.

Conversely, the Cr isotope variation observed in lunar magmas is larger, up to 0.22‰. Lunar mare basalt parent magmas have Mg# ~ 0.45, constrained by Fo_{72} and a $K^{Fe-Mg}_{Dol-melt} = 0.3$ (37). These magmas have 1 bar liquidus temperatures of ~1,200–1,250 °C, at which point olivine and chromite crystallize in tandem (38). The Cr isotopic fractionation between Cr^{3+}-bearing chromite and a lunar silicate melt (assuming it is equivalent to Cr^{2+}-bearing forsterite) with $Cr^{2+}/\sum Cr = 0.91$ is $+0.35 \times 10^6/T^2$ (39), or $\Delta^{53}Cr_{chromite-melt} = +0.16$‰ at 1,200 °C, which is identical to that empirically determined by ref. 31.

The cumulate samples of the Mg Suite, whose compositions are complementary to those of liquids, have a more magnesian parent magma (~13 wt% MgO; refs. 40 and 41) than those of mare basalts, with a higher liquidus (1,300 °C), at which only olivine is stable. Indeed, the Cr budget in 72415 dunite and 76535 troctolite was entirely hosted in olivine (41), into which both Cr^{2+} and Cr^{3+} are incorporated subequally. Thus, minimal isotopic fractionation occurs during crystallization of 72415 and 76535, meaning that their Cr isotope composition reflects that of the Mg-Suite parent magma. Relative to Cr^{2+}, trivalent Cr is ~10 times more compatible in orthopyroxene (35), such that even a lunar melt with ~10% Cr^{3+} will crystallize orthopyroxene with $Cr^{2+}/\sum Cr \sim 0.45$. Adopting $\Delta^{53}Cr_{Cr3+-Cr2+} = +0.35 \times 10^6/T^2$ (39), weighted for the difference in $Cr^{2+}/\sum Cr$ between orthopyroxene and melt, predicts $\Delta^{53}Cr_{opx-melt} = +0.10$‰ at 1,200 °C
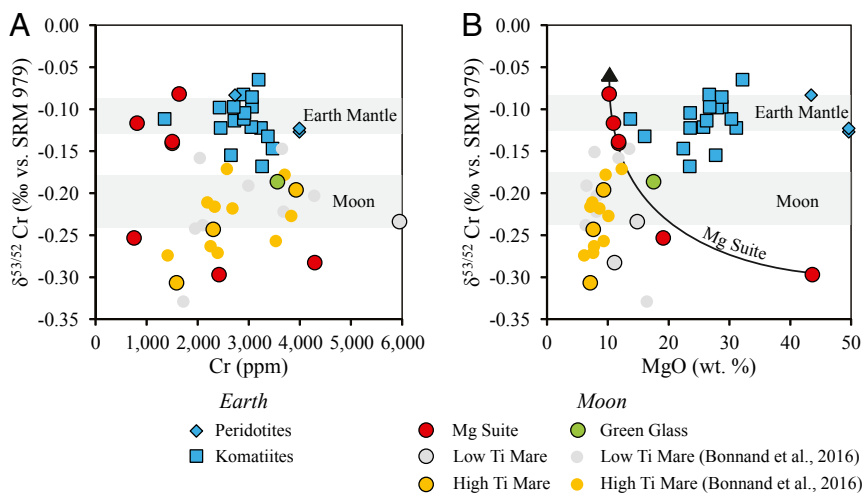
Fig. 1. The chromium isotope composition, expressed as $\delta^{53}Cr$, of lunar samples; Mg Suite, red ($n = 6$); green glass, green ($n = 1$); high Ti, yellow ($n = 13$); low Ti, gray ($n = 11$); smaller circles show the data of ref. 30; and terrestrial komatiites (blue squares, $n = 17$) and peridotites (blue diamonds, $n = 3$) as a function of their chromium (A) and MgO (B) content. Also shown are a trend line for the Mg Suite (black line) and estimates for the bulk composition of BSE (Earth Mantle) and the Moon (gray fields).

(*SI Appendix*, Fig. S1). This results in orthopyroxene-plagioclase cumulates, represented by norites 78235/8 and the more evolved 15455, with $\delta^{53}Cr$ 0.10‰ heavier than the Mg-Suite parent magma ($-0.25‰$), in agreement with the measured values (Table 1). Norite 15445 is mineralogically similar to 15455, except that it has twice the amount of Cr (1,635 vs. 810 ppm) and a correspondingly heavier $\delta^{53}Cr$ ($-0.08 \pm 0.01‰$ vs. $-0.12 \pm 0.01‰$), consistent with 0.25% chromite accumulation.

Composition of the BSE and Moon

Owing to the potential for chromite to engender isotopic fractionation, especially in lunar magmas where the disparity in valence state of Cr in the melt (Cr^{2+}) and in chromite (Cr^{3+}) is large, quenched liquids or direct mantle samples are the best indicators of mantle composition.

In determining the Cr isotope composition of the BSE, data for ultramafic rocks from this study and the literature (30, 42, 43) were filtered for (i) lithologies that represent mantle-derived rocks (excluding cumulates such as wehrlites and hornblendites) and (ii) fertile, unmetasomatized peridotites with Cr contents of $2,520 \pm 630$ ppm, Mg# [molar Mg/(Mg+Fe)] between 0.885 and 0.910, and >2 wt% Al_2O_3. The remaining 42 samples with mean $\delta^{53}Cr = -0.11 \pm 0.11‰$ were then filtered for statistical outliers at the 95% confidence level using Grubbs' test, leaving 36 samples with $\delta^{53}Cr = -0.11 \pm 0.06‰$, whose population is normally distributed (*SI Appendix*, Table S9) and has a 2SE of $\pm 0.02‰$.

To quantify the degree of mineral accumulation in lunar mare basalts, bulk rock Mg# was compared with that expected for a liquid in equilibrium with the highest Mg# olivine (or orthopyroxene in olivine-free basalts) in the sample, given $K_{Dol,opx-melt}^{Fe-Mg} \sim 0.3$ (44). Samples were rejected from the derivation of the bulk silicate Moon value if they had experienced (i) significant (>0.1) olivine accumulation or fractionation ($0.4 < $ Mg# < 0.5 were kept) and (ii) chromite accumulation (high Cr and $\delta^{53}Cr$) or fractionation (low Cr and $\delta^{53}Cr$). This exercise left 17 measurements of 15 lunar samples from ref. 31 and this study, with average $\delta^{53}Cr = -0.21 \pm 0.06‰$ and 2SE of $\pm 0.03‰$ (*SI Appendix*, Table S11; no outliers were found).

A two-tailed Student's *t* test yielded a *t* statistic of 13.36 relative to a critical value of 2.00, illustrating that the $\delta^{53}Cr$ of the Earth ($-0.11 \pm 0.02‰$, 2SE, $n = 36$) and Moon ($-0.21 \pm 0.03‰$, 2SE, $n = 17$) are clearly statistically resolvable at $\Delta^{53}Cr_{Moon-Earth} = -0.10 \pm 0.04‰$.

Estimates for the Cr content of the lunar mantle, based on Fe/Cr and on Cr/V correlations in lunar rocks give 2,200 and 2,500 ppm (8), respectively. The latter estimate is a maximum because it assumes V is refractory, despite the fact that Al/V ratios increase from 159 in CI chondrites to 182 in CV chondrites (9). If V is slightly depleted in the Moon (by a factor of 159/182),

then its Cr content decreases to 2,180 ppm. A value of 2,000 ppm is calculated by combining the $\sim$3,500 ppm Cr in lunar green glass beads with chromium partitioning during partial melting of an olivine-dominated lunar mantle source (9). An average of these estimates gives $2,125 \pm 110$ ppm Cr in the Moon, which is therefore depleted with respect to the Earth's mantle ($2,520 \pm 250$ ppm) by $16 \pm 10\%$.

Isotopic Fractionation of Chromium During Planetary Formation

By adopting the Earth's mantle as the Moon's progenitor (4, 40), either core formation or volatile loss can simultaneously decrease Cr abundance and shift its isotopic composition.

Geophysical results from the Gravity Recovery and Interior Laboratory mission have shown that the core comprises 1% of the Moon's mass (45). At 55 kbar, the pressure at its center, the partition coefficient of Cr into Fe–Ni metal is very near unity at IW-2 (10), and, as such, the lunar core would only contribute to a minor ($\sim$1%) depletion of Cr, attested to by the paucity of solutions in lunar core formation models that fit observed Cr depletion (46). Furthermore, ab initio calculations show that the isotopic composition of metallic Cr is slightly lighter than Cr^{2+} in the M sites of olivine (39), meaning that metal segregation would result in isotopically heavy silicates, contrary to observations. It is therefore unlikely that core formation can account for the Cr depletion or its light isotopic composition in the lunar mantle.

Vaporization of silicate material of a bulk lunar composition gives rise to fO_2 of IW+2.5 at 1,800 K (13). The relatively oxidizing vapor, near the FMQ buffer, evolved upon evaporation of silicate material, be it at high temperature (1,827–1,970 K, olivine; ref. 47) or low temperature (1,396–1,499 K, lunar mare basalt 12002; ref. 48) is evidenced by experimental Knudsen effusion mass spectrometry studies. Gas-phase equilibria among the four Cr oxide species (ref. 27 and *SI Appendix*, Fig. S2) show that $CrO_{2(g)}$ is stable for all $fO_2 >$ IW. Considering the predominance of Cr^{2+} in a lunar silicate liquid (34), the appropriate evaporation equation is:

$$CrO(l) + \frac{1}{2}O_2 = CrO_2(g). \qquad [2]$$
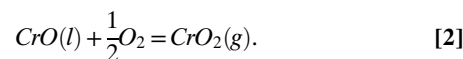
Increasing oxygen fugacity increases the volatility of Cr (Eq. **2**), in contrast to Zn, Rb, Ga, or K (25). The partial pressure of $CrO_{2(g)}$ is calculated in a vapor in equilibrium with a BSE-like silicate melt composition (13) as a function of temperature and fO_2 (Fig. 2). Given an ideal gas, significant (>1%) Cr in the vapor occurs only above 1,500 K (Fig. 2), assuming a CrO activity coefficient in silicate melts of $\sim$3 (34).
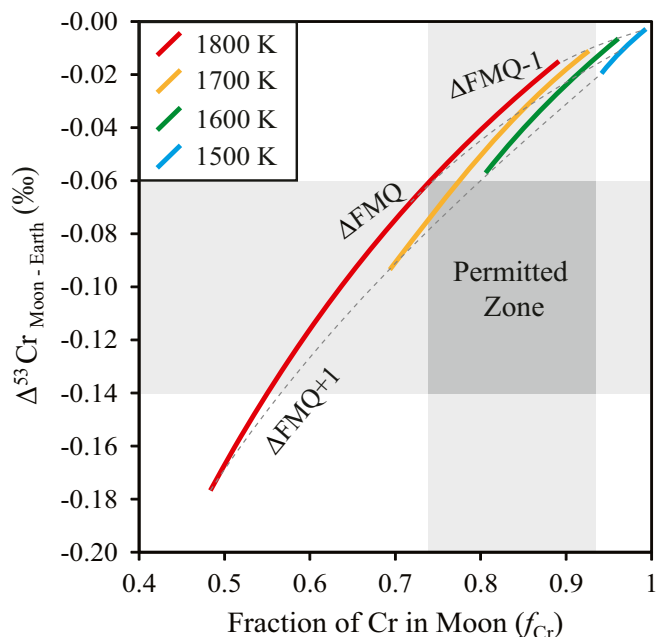
Fig. 2. The fraction of Cr remaining in the bulk silicate Moon relative to the BSE, f_{Cr}, as a function of the $\delta^{53/52}Cr$ isotopic difference between the Moon and BSE, $\Delta^{53}Cr_{Moon-Earth}$. The curves correspond to values of f_{Cr} and $\Delta^{53}Cr_{Moon-Earth}$ calculated by liquid–vapor equilibrium between $CrO_2(g)$ and $CrO(l)$ at various temperatures (1,500 K, blue; 1,600 K, green; 1,700 K, yellow; and 1,800 K, red) and oxygen fugacities (dashed lines, ΔFMQ+1, ΔFMQ, and ΔFMQ-1). Values of f_{Cr} are calculated from Eq. **2** and depend on temperature, pressure, and fO_2, where the total pressure is that in the gas above a BSE composition (13). Values of $\Delta^{53}Cr_{Moon-Earth}$ are given by Eq. **4**. The dark gray field demarcates the permissible range of f_{Cr} and $\Delta^{53}Cr_{Moon-Earth}$ defined by sample data; curves passing through this field satisfy both constraints.

Whether gas–liquid exchange between $CrO_{2(g)}$ and $CrO_{(l)}$ can drive the condensed phase to isotopically light compositions requires knowledge of the force constants of Cr–O bonds in both $CrO_{(l)}$ and $CrO_{2(g)}$, neither of which are available. To remedy this, we calculated the reduced partition function ratio of $^{53}Cr/^{52}Cr$ substitution in the diatomic molecule $CrO_{(g)}$ in the harmonic approximation (49), given the Cr–O vibrational frequency of 864 cm^{-1} (50). Then, bond valence theory was used in the electrostatic description of bonding with Born–Landé potentials (51) to predict the mean bond strength of $CrO_{(g)}$. $CrO_{2(g)}$, and $CrO_{3(g)}$, giving $10^3\ln\beta^{53/52}Cr$ of 0.28, 0.57, and 0.89 × $10^6/T^2$, respectively (*SI Appendix*, Fig. S3 and Table S12). This approach yields force constants that agree with spectroscopic or experimental determinations to within 50% (×$10^6/T^2$). By using the $10^3\ln\beta^{53/52}Cr$ of the Cr_2SiO_4 component in olivine, 0.26 × $10^6/T^2$, as an analog for $CrO_{(l)}$ (39), the $^{53}Cr/^{52}Cr$ isotope fractionation factor for Eq. **2** may be written:

$$\Delta^{53}Cr_{CrO(l)-CrO_2(g)} = -0.31 \pm 0.16 \times \frac{10^6}{T^2} (\%o). \quad [3]$$

The composition of the lunar mantle in equilibrium with a CrO_2-bearing gas phase can be calculated by mass balance, in which:

$$\delta^{53}Cr_{vapor} = \frac{\delta^{53}Cr_{system} - \delta^{53}Cr_{silicate\ moon} f_{silicate\ moon}^{Cr}}{\left(1 - f_{silicate\ moon}^{Cr}\right)}. \quad [4]$$

The $\delta^{53}Cr_{system}$ is Earth's mantle (−0.11 ± 0.02‰), $\delta^{53}Cr_{silicate\ moon}$ is −0.21 ± 0.03‰, and $f_{silicate\ moon}^{Cr}$ is 0.84 ± 0.10, yielding $\delta^{53}Cr_{vapor}$ = +0.41 ± 0.33‰ or (+2.00/−0.45)‰, considering uncertainty in the Cr depletion in the lunar mantle. Solving Eq. **3** for temperature and

propagating uncertainties yields ~700 (+1,100/−300) K. Importantly, both thermodynamic and isotopic constraints converge at temperatures between 1,600 and 1,800 K and fO_2 between FMQ and FMQ+1 (Fig. 2).

Implications for the Origin of the Moon

Relative to terrestrial ultramafic rocks, the uniformly light Cr isotope composition of samples most representative of the lunar mantle, independent of whether they are extrusive (e.g., green glass) or intrusive (Mg Suite) supports a global-scale vapor-loss event, manifest in the depletion of moderately volatile elements (2, 4, 11). In contrast with recent numerical giant impact models that predict temperatures >4,000 K (15, 52), the temperature of volatile loss must have been <1,800 K to produce measurable equilibrium isotope fractionation of Cr (Fig. 2). Moreover, Zn, Ga, and Cl exhibit variable isotopic compositions in different lithologies, suggesting that lunar volatile loss occurred during magma ocean crystallization, at temperatures not higher than the silicate liquidus (23, 24). If volatile depletion did occur as a direct result of the impact, evaporation at the highest temperatures did not leave any stable isotopic trace. Instead, isotopic fractionation and loss must have occurred after the Earth–Moon system had fallen from its peak temperatures.

This is difficult to reconcile with the supposition that loss of a volatile-laden atmosphere is facilitated by higher temperatures (T), which impart higher velocities on its constituent particles (v_{th}) of mass m, such that more exceed the escape velocity of a body (v_{esc}), a condition that is quantified by the escape parameter (53):

$$\lambda_{esc} = \frac{mv_{esc}^2}{2k_BT}, \quad [5]$$

where a value of approximately three marks the transition between the Jeans (greater than three) and Hydrodynamic (less than three) escape regimes. Given that the temperature of the atmosphere decays over time, $t_{1/2} \sim 100$ y (54, 55), the likelihood of gas escape should be highest immediately after the giant impact (Eq. **5**). However, the v_{esc} of a body is proportional to its mass. Before the accretion of the Moon, the bulk of the material lies within the Roche limit (Fig. 3A and ref. 56), where the combined masses of the Earth and Moon result in high v_{esc} (11.2 km/s), thereby rendering volatile escape difficult, especially in the presence of an O_2- and SiO-dominated vapor (57). Indeed, at 4,000 K, 99.99% of molecules (m = 0.052 kg/mol) in the vapor have v_{th} < 3.8 km/s. However, as the disk cools, material migrates beyond the Roche limit by viscous spreading and begins to form the proto-Moon within 1,000 y of the initial collision (Fig. 3B and ref. 55). Over this time, the disk has cooled sufficiently to temperatures (54) that are consistent with estimates based on Cr isotopes (1,600–1,800 K; Fig. 3C). The formation of the Moon facilitates volatile escape due to the decrease in escape velocity compared with that of Earth. A particle is lost from the Moon's atmosphere when it is trapped by the gravity field of Earth, at a boundary called the Hill sphere, and is:

$$v_{esc,\ Moon(Hill)} = \sqrt{2GM_{Moon}\left(\frac{1}{r} - \frac{1}{r_H}\right)}, \quad [6]$$

where G is the gravitational constant, M and r are the Moon's mass and radius, and r_H is the Hill sphere radius [$r_H = a(M_M/3M_E)^{1/3}$], where a is the distance between M_M and M_E (taken to be the Roche limit, $3R_E$). Gaseous molecules in the atmosphere surrounding the Moon have a Maxwell–Boltzmann distribution of velocities for which 2% (1,600 K) to 4% (1,800 K) exceed the Hill escape velocity of the Moon. In this scenario, $\lambda_{esc} \sim 4$–5, meaning that loss of Cr from the lunar atmosphere is expected to occur via Jeans escape. Continued outward migration of the Moon beyond $3R_E$ increases v_{esc} (Eq. **6**) and hence λ_{esc}. If Jeans escape controlled the lunar abundances and stable isotope compositions of the
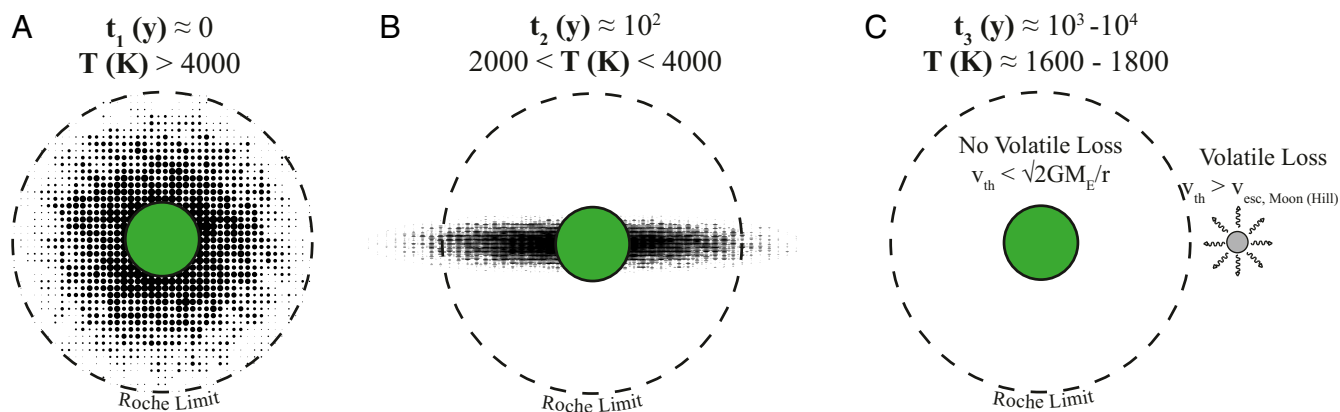
Fig. 3. A schematic illustration of the timing and conditions of events following a giant impact. (*A*) t_1, 0 y A hot (>4,000 K) gas- and dust-rich vapor envelope surrounds the proto-Earth within its Roche limit. At 4,000 K, >99.99% of the volatile species of molar mass 0.052 kg/mol have $v_{th} < 3.8$ km/s, significantly lower than the 11.2 km/s v_{esc} of Earth, preventing any volatile escape of Cr. (*B*) As the disk cools, the vapor disk rotates, settles, and spreads along the midplane, exceeding the Roche limit over a period of ~100 y. (*C*) The material outside the Roche limit is able to condense and accrete to form the Moon. At this point, the temperature has fallen to 1,600–1,800 K, and the remaining gas particles have a Maxwell–Boltzmann distribution of velocities, 2–4% of which exceed the escape velocity of the Moon at a given time, which is calculated to occur at the Hill radius at 3 R_E to be 1.56 km/s and are lost over the timescale of years.

moderately volatile elements, their fractionation should depend on $(m_1/m_2)^{0.5}$, causing them to be isotopically heavy in the Moon. This is difficult to uniquely assess for elements like Zn or K (17, 18) because a combination of both equilibrium and kinetic isotope fractionation induced by Jeans escape could have produced the heavy isotopic compositions observed. Conversely, that Cr isotopes are lighter in the Moon relative to Earth implies that volatile loss via Jeans escape was either unimportant (i.e., loss was driven by another process) or went to completion, resulting in quantitative loss of the Cr (and lighter elements) present in the lunar atmosphere over the timescales for cooling of the Moon.

Materials and Methods

Chromium Double Spike. A ^{50}Cr–^{54}Cr double spike was prepared from enriched ^{50}Cr (96.5%; oxide form) and ^{54}Cr (95.5%; metal form), purchased from CortecNet. The single spikes were separately digested in 6 M HCl at ~120 °C on a hotplate (^{54}Cr) and in 15 M HNO$_3$ in a Parr Bomb at ~160 °C for several days (^{50}Cr), respectively. After digestion, the ^{54}Cr was evaporated and redissolved in 15 M HNO$_3$. The optimal spike composition (i.e., 0.58:0.42 ^{50}Cr:^{54}Cr) was calculated by using the double spike toolbox (58). The two digested single spikes were mixed accordingly, and the double spike was further diluted with 2 M HNO$_3$ to a concentration of ~38 μg/mL The ^{50}Cr–^{54}Cr double spike was calibrated relative to the reference material NIST SRM 979 for spike:sample mixing ratios of 0.13:0.87 to 0.39:0.61. The optimal mixing ratio according to ref. 58 is 0.28:0.72.

Sample Preparation and Purification. Approximately 30 mg of sample powder was dissolved in a concentrated HCl–HF–HNO$_3$ mixture (1, 0.5, and 0.2 mL, respectively) at 130 °C for 48 h and afterward evaporated. Subsequently, the samples were redissolved in concentrated HNO$_3$–HF (2 and 0.2 mL, respectively) and placed in Parr Bombs under pressurized steel jackets at 190 °C in an oven for 72 h to dissolve refractory chromite. No residues were observed upon visual inspection of the digested samples. An adequate amount of ^{50}Cr–^{54}Cr double spike was added to the samples following dissolution, and sample and double spike were allowed to equilibrate in closed perfluoroalkoxy alkane (PFA) Teflon sample vials at ~120 °C overnight. Chemical separation of Cr from matrix elements (e.g., Mg, Ca, and Fe), and particularly from elements causing isobaric interferences on the Cr masses during mass spectrometry (i.e., Fe, Ti, and V), was achieved by using a two-step chromatography procedure with AG50W-X8 (200–400 mesh) cation exchange resin, adapted from ref. 59. The first cation-exchange column, custom-made from heat-shrinkable Teflon, accommodated 1.1 mL of resin and was conditioned with 0.5 M HCl. Evaporated samples were redissolved and loaded in 1.1 mL of 0.55 M HCl, and Cr was collected immediately upon sample loading. Further elution of Cr was achieved in 4 mL of 1 M HCl. Major matrix elements, such as Mg, Ca, and Fe, remained sorbed to the resin, quantitatively removing them from the Cr-bearing eluate during this step. As minor amounts

of Al, Ti, and V coelute with Cr, a second cation-exchange column was used to further purify the samples. The evaporated Cr fraction was redissolved in 2.1 mL of 0.8 M HNO$_3$ and loaded onto custom-made Teflon microcolumns, accommodating 300 μL of cation-exchange resin, which was conditioned with MilliQ deionized H$_2$O. Matrix elements were removed with 2.5 mL of 0.8 M HF and 6 mL of 1 M HCl before Cr was collected in 3 mL of 6 M HCl. Recovery of Cr from this procedure was between 60% and 90%. Although stable isotope fractionation is caused by incomplete elution of Cr (42), this, along with other sources of mass bias during analysis, was corrected for by the double spike reduction. Following chromatographic purification, the samples were evaporated under concentrated HNO$_3$, diluted to a concentration of 1 ppm Cr, and dissolved in 2% (vol/vol) (0.317 M) HNO$_3$ for isotope analysis.

Mass Spectrometry and Data Reduction. The purified Cr samples were introduced via a Cyclonic-Scott Double Pass spray chamber into a Thermo Scientific Neptune Plus multicollector inductively coupled plasma mass spectrometer housed at the Institut de Physique du Globe de Paris. Medium-resolution mode, which permits resolution of polyatomic interferences (e.g., ^{40}Ar^{14}N$^+$ on ^{54}Cr$^+$ and ^{40}Ar^{16}O$^+$ on ^{56}Fe$^+$) was employed, and analyses were performed on peak shoulders. Isobaric interferences from ^{54}Fe$^+$ on ^{54}Cr$^+$ and ^{50}Ti$^+$ and ^{50}V$^+$ on ^{50}Cr$^+$ were monitored on ^{56}Fe$^+$, ^{49}Ti$^+$, and ^{51}V$^+$, respectively, and corrected for by using the exponential mass fractionation law. Samples were bracketed by the NIST SRM 979 reference material (standard-sample-sample-standard) and analyzed two or three times each, with each analysis consisting of 100 cycles of 4.194-s integration time. Instrumental mass bias was corrected for by the ^{50}Cr–^{54}Cr double spike, following the iterative solution of ref. 60, assuming exponential instead of linear fractionation. The isotopic ratio is reported in delta notation:

$$\delta^{53}Cr(‰) = \left(\frac{\left(^{53}Cr/^{52}Cr\right)_{sample}}{\left(^{53}Cr/^{52}Cr\right)_{NIST\ SRM\ 979}} - 1 \right) \times 1,000. \qquad [7]$$

The intermediate measurement precision was estimated by calculating the pooled SD (s_p) of the sample dataset:

$$s_p = \sqrt{\frac{\sum_{i=1}^{k}(n_i - 1)s_i^2}{\sum_{i=1}^{k}(n_i - 1)}}, \qquad [8]$$

where n_i is the number of repeated measurements of each sample i and s_i^2 their variance. The resulting $2s_p$ of ±0.03‰ ($k = 35$) is identical to the 2SD of repeated analyses of the US Geological Survey geological reference material BHVO-2 ($-0.104 \pm 0.03‰$; $n = 4$). The δ^{53}Cr value of the BHVO-2 is further in agreement with literature data (61–63), assuring accuracy of the analyses.

Sossi et al.

1. Ringwood AE, Essene E (1970) Petrogenesis of Apollo 11 basalts, internal constitution and origin of the moon. *Proceedings of the Apollo 11 Lunar Science Conference* (Pergamon Press, New York), pp 769–799.
2. Taylor SR, Taylor GJ, Taylor LA (2006) The moon: A Taylor perspective. *Geochim Cosmochim Acta* 70:5904–5918.
3. Day JMD, Moynier F (2014) Evaporative fractionation of volatile stable isotopes and their bearing on the origin of the Moon. *Philos Trans A Math Phys Eng Sci* 372: 20130259.
4. Ringwood AE, Kesson SE (1977) Basaltic magmatism and the bulk composition of the moon. *Moon* 16:425–464.
5. Zhang J, Dauphas N, Davis AM, Leya I, Fedkin A (2012) The proto-Earth as a significant source of lunar material. *Nat Geosci* 5:251–255.
6. Mougel B, Moynier F, Göpel C (2018) Chromium isotopic homogeneity between the Moon, the Earth, and enstatite chondrites. *Earth Planet Sci Lett* 481:1–8.
7. Dauphas N, Burkhardt C, Warren PH, Teng F-Z (2014) Geochemical arguments for an Earth-like Moon-forming impactor. *Philos Trans A Math Phys Eng Sci* 372:20130244.
8. Seifert S, Ringwood AE (1988) The lunar geochemistry of chromium and vanadium. *Earth Moon Planets* 40:45–70.
9. Jones JH, Palme H (2000) Geochemical constraints on the origin of the Earth and Moon. *The Origin of the Earth and Moon*, eds Canup RM, Righter K (Univ of Arizona Press, Tucson, AZ), pp 197–216.
10. Siebert J, Badro J, Antonangeli D, Ryerson FJ (2013) Terrestrial accretion under oxidizing conditions. *Science* 339:1194–1197.
11. O'Neill HSC (1991) The origin of the Moon and the early history of the Earth—A chemical model. Part 1: The Moon. *Geochim Cosmochim Acta* 55:1135–1157.
12. Newsom HE, Taylor SR (1989) Geochemical implications of the formation of the Moon by a single giant impact. *Nature* 338:29–34.
13. Visscher C, Fegley B, Jr (2013) Chemistry of impact-generated silicate melt-vapor debris disks. *Astrophys J* 767:L12.
14. Canup RM, Visscher C, Salmon J, Fegley B, Jr (2015) Lunar volatile depletion due to incomplete accretion within an impact-generated disk. *Nat Geosci* 8:1–6.
15. Lock SJ, et al. (2018) The origin of the Moon within a terrestrial synestia. *J Geophys Res Planets* 123:910–951.
16. Paniello RC, Day JMD, Moynier F (2012) Zinc isotopic evidence for the origin of the Moon. *Nature* 490:376–379.
17. Kato C, Moynier F, Valdes MC, Dhaliwal JK, Day JMD (2015) Extensive volatile loss during formation and differentiation of the Moon. *Nat Commun* 6:7617.
18. Wang K, Jacobsen SB (2016) Potassium isotopic evidence for the origin of the moon. *Nature* 538:487–490.
19. Pringle EA, Moynier F (2017) Rubidium isotopic composition of the Earth, meteorites, and the Moon: Evidence for the origin of volatile loss during planetary accretion. *Earth Planet Sci Lett* 473:62–70.
20. Sharp ZD, Shearer CK, McKeegan KD, Barnes JD, Wang YQ (2010) The chlorine isotope composition of the moon and implications for an anhydrous mantle. *Science* 329:1050–1053.
21. Kato C, Moynier F (2017) Gallium isotopic evidence for extensive volatile loss from the Moon during its formation. *Sci Adv* 3:e1700571.
22. O'Hara M, Biggar GM, Richardson SW, Ford CE, Jamieson BG (1970) The nature of seas, mascons and the lunar interior in the light of experimental studies. *Proceedings of the Apollo 11 Lunar Science Conference* (Pergamon Press, New York), pp 695–710.
23. Dhaliwal JK, Day JMD, Moynier F (2018) Volatile element loss during planetary magma ocean phases. *Icarus* 300:249–260.
24. Boyce JW, et al. (2015) The chlorine isotope fingerprint of the lunar magma ocean. *Sci Adv* 1:e1500380.
25. Lamoreaux RH, Hildenbrand DL, Brewer L (1987) High-temperature vaporization behavior of oxides II. Oxides of Be, Mg, Ca, Sr, Ba, B, Al, Ga, In, Tl, Si, Ge, Sn, Pb, Zn, Cd, and Hg. *J Phys Chem Ref Data* 16:419–443.
26. Ducher M, Blanchard M, Balan E (2016) Equilibrium zinc isotope fractionation in Zn-bearing minerals from first-principles calculations. *Chem Geol* 443:87–96.
27. Chase MW (1998) *NIST-JANAF thermochemical tables*. Journal of Physical and Chemical Reference Data Monograph (National Institute of Standards and Technology, Gaithersburg, MD), No. 9 (Parts I and II), 4th Ed.
28. Sossi PA, et al. (2016) Petrogenesis and geochemistry of Archean komatiites. *J Petrol* 57:147–184.
29. Shearer CK, Elardo SM, Petro NE, Borg LE, McCubin FM (2015) Origin of the lunar highlands Mg-Suite: An integrated petrology, geochemistry, chronology, and remote sensing perspective. *Am Mineral* 100:294–325.
30. Schoenberg R, et al. (2016) The stable Cr isotopic compositions of chondrites and silicate planetary reservoirs. *Geochim Cosmochim Acta* 183:14–30.
31. Bonnand P, Parkinson IJ, Anand M (2016) Mass dependent fractionation of stable chromium isotopes in mare basalts: Implications for the formation and the differentiation of the Moon. *Geochim Cosmochim Acta* 175:208–221.
32. Li J-P, O'Neill HSC, Seifert F (1995) Subsolidus phase relations in the system MgO-SiO2-Cr-O in equilibrium with metallic Cr, and their significance for the petrochemistry of chromium. *J Petrol* 36:107–132.
33. Herd CDK (2008) Basalts as probes of planetary interior redox state. *Reviews in Mineralogy and Geochemistry: Oxygen in the Solar System*, ed MacPherson GJ (Mineralogical Society of America, Washington, DC), 68th Ed, pp 527–553.
34. Berry AJ, O'Neill HSC, Scott DR, Foran GJ, Shelley JMG (2006) The effect of composition on Cr^{2+}/Cr^{3+} in silicate melts. *Am Mineral* 91:1901–1908.
35. Barnes SJ (1986) The distribution of chromium among orthopyroxene, spinel and silicate liquid at atmospheric pressure. *Geochim Cosmochim Acta* 50:1889–1909.
36. Sossi PA, O'Neill HSC (2016) Liquidus temperatures of komatiites and the effect of cooling rate on element partitioning between olivine and komatiitic melt. *Contrib Mineral Petrol* 171:1–25.
37. Beaty DW, Albee AL (1978) Comparative petrology and possible genetic relations among the Apollo 11 basalts. *Proceedings of the Lunar and Planetary Science Conference, 9th* (Pergamon Press, New York), pp 359–463.
38. Longhi J (1992) Experimental petrology and petrogenesis of mare volcanics. *Geochim Cosmochim Acta* 56:2235–2251.
39. Moynier F, Yin Q-Z, Schauble E (2011) Isotopic evidence for Cr partitioning into Earth's core. *Science* 331:1417–1420.
40. Sossi PA, Moynier F (2017) Chemical and isotopic kinship of iron in the Earth and Moon deduced from the lunar Mg-Suite. *Earth Planet Sci Lett* 471:125–135.
41. McCallum IS, Schwartz JM (2001) Lunar Mg Suite: Thermobarometry and petrogenesis of parental magmas. *J Geophys Res* 106:27969.
42. Schoenberg R, Zink S, Staubwasser M, von Blanckenburg F (2008) The stable Cr isotope inventory of solid Earth reservoirs determined by double spike MC-ICP-MS. *Chem Geol* 249:294–306.
43. Xia J, et al. (2017) Chromium isotope heterogeneity in the mantle. *Earth Planet Sci Lett* 464:103–115.
44. Longhi J, Walker D, Hays JF (1978) The distribution of Fe and Mg between olivine and lunar basaltic liquids. *Geochim Cosmochim Acta* 42:1545–1558.
45. Wieczorek MA, et al. (2013) The crust of the Moon as seen by GRAIL. *Science* 339:671–675.
46. Steenstra ES, Rai N, Knibbe JS, Lin YH, van Westrenen W (2016) New geochemical models for core formation in the Moon from metal–silicate partitioning of 15 siderophile elements. *Earth Planet Sci Lett* 441:1–9.
47. Costa GCC, Jacobson NS, Fegley B (2017) Vaporization and thermodynamics of forsterite-rich olivine and some implications for silicate atmospheres of hot rocky exoplanets. *Icarus* 289:42–55.
48. De Maria G, Balducci G, Guido M, Piacente V (1971) Mass spectrometric investigation of the vaporization process of Apollo 12 lunar samples. *Proceedings of Second Lunar Science Conference* (MIT Press, Cambridge, MA), Vol 2, pp 1367–1380.
49. Schauble EA (2004) Applying stable isotope fractionation theory to new systems. *Reviews in Mineralogy and Geochemistry: Geochemistry of Non-Traditional Stable Isotopes*, eds Johnson CM, Beard BL, Albaréde F (Mineralogical Society of America, Washington, DC), 55th Ed, pp 65–111.
50. Espelid O, Borve KJ, Jensen VR (1998) Structure and thermodynamics of gaseous oxides, hydroxides, and mixed oxohydroxides of chromium: $CrO_m(OH)_{(n)}$ (m, n = 0-2) and CrO_3. A computational study. *J Phys Chem A* 102:10414–10423.
51. Sossi PA, O'Neill HSC (2017) The effect of bonding environment on iron isotope fractionation between minerals at high temperature. *Geochim Cosmochim Acta* 196:121–143.
52. Nakajima M, Stevenson DJ (2015) Melting and mixing states of the Earth's mantle after the Moon-forming impact. *Earth Planet Sci Lett* 427:286–295.
53. Genda H, Abe Y (2003) Modification of a proto-lunar disk by hydrodynamic escape of silicate vapor. *Earth Planets Space* 53:53–57.
54. Pritchard ME, Stevenson DJ (2000) Thermal aspects of a lunar origin by giant impact. *The Origin of the Earth and Moon*, eds Canup RM, Righter K (Univ of Arizona Press, Tucson, AZ), pp 179–196.
55. Charnoz S, Michaut C (2015) Evolution of the protolunar disk: Dynamics, cooling timescale and implantation of volatiles onto the Earth. *Icarus* 260:440–463.
56. Ida S, Canup RM, Stewart GR (1997) Lunar accretion from an impact-generated disk. *Nature* 389:353–357.
57. Nakajima M, Stevenson DJ (2018) Inefficient volatile loss from the Moon-forming disk: Reconciling the giant impact hypothesis and a wet Moon. *Earth Planet Sci Lett* 487:117–126.
58. Rudge JF, Reynolds BC, Bourdon B (2009) The double spike toolbox. *Chem Geol* 265:420–431.
59. Trinquier A, Birck J-L, Allègre CJ (2008) High-precision analysis of chromium isotopes in terrestrial and meteorite samples by thermal ionization mass spectrometry. *J Anal At Spectrom* 23:1565–1574.
60. Compston W, Oversby VM (1969) Lead isotopic analysis using a double spike. *J Geophys Res* 74:4338–4348.
61. Cole DB, et al. (2016) A shale-hosted Cr isotope record of low atmospheric oxygen during the Proterozoic. *Geology* 44:555–558.
62. Wang X, et al. (2016) Chromium isotope fractionation during subduction-related metamorphism, black shale weathering, and hydrothermal alteration. *Chem Geol* 423:19–33.
63. Gueguen B, et al. (2016) The chromium isotope composition of reducing and oxic marine sediments. *Geochim Cosmochim Acta* 184:1–19.

EARTH, ATMOSPHERIC, AND PLANETARY SCIENCES